12-2022

Statistical Analysis of Aquifer Hydraulic Properties by a Continuous Pumping Tomography Test: Application to the Boise Hydrogeophysical Research Site

Kan Bun Cheng
Tel-Aviv University

Gedeon Dagan
Tel-Aviv University

Warren Barrash
Boise State University

Michael Cardiff
University of Wisconsin-Madison

Avinoam Rabinovich
Tel-Aviv University

Publication Information

Cheng, Kan Bun; Dagan, Gedeon; Barrash, Warren; Cardiff, Michael; and Rabinovich, Avinoam. (2022). "Statistical Analysis of Aquifer Hydraulic Properties by a Continuous Pumping Tomography Test: Application to the Boise Hydrogeophysical Research Site". *Water Resources Research, 58*(12), e2022WR032464. https://doi.org/10.1029/2022WR032464

AGU ADVANCING EARTH AND SPACE SCIENCE

Water Resources Research

RESEARCH ARTICLE

10.1029/2022WR032464

Key Points:

- New approach for statistical analysis of equivalent hydraulic properties (conductivity, specific storage, and specific yield) is presented
- Method is applied to tomographic pumping test data from the Boise aquifer to find mean and variance of equivalent properties
- The mean is shown to decrease with distance from pumping well and appears to converge to the effective value at a distance

Correspondence to:

A. Rabinovich,
avinoamr@tauex.tau.ac.il

Citation:

Cheng, K. B., Dagan, G., Barrash, W., Cardiff, M., & Rabinovich, A. (2022). Statistical analysis of aquifer hydraulic properties by a continuous pumping tomography test: Application to the Boise Hydrogeophysical Research Site. *Water Resources Research*, *58*, e2022WR032464. https://doi.org/10.1029/2022WR032464

Received 31 MAR 2022
Accepted 19 NOV 2022

Statistical Analysis of Aquifer Hydraulic Properties by a Continuous Pumping Tomography Test: Application to the Boise Hydrogeophysical Research Site

Kan Bun Cheng[1], Gedeon Dagan[1], Warren Barrash[2], Michael Cardiff[3], and Avinoam Rabinovich[1]

[1]School of Mechanical Engineering, Tel-Aviv University, Tel-Aviv, Israel, [2]Department of Geosciences, Boise State University, Boise, ID, USA, [3]Department of Geoscience, University of Wisconsin-Madison, Madison, WI, USA

Abstract Characterizing aquifer heterogeneity is paramount for accurate flow and transport modeling. In this work, we present a new approach for statistical analysis of hydraulic properties in continuous pumping tomography tests of a phreatic aquifer. The method entails determining equivalent hydraulic conductivity (K_{eq}), specific storage ($S_{s,eq}$), and specific yield ($S_{y,eq}$) at many locations in the field and then calculating statistical moments of the equivalent properties, assuming they are random space variables. Equivalent properties are defined as the ones pertinent to a homogeneous aquifer for which the head time dependent signal fits the one observed in the pumping test. Calculation is carried out in a novel approach, by matching measured head data to two separate semianalytical solutions considering two time periods, early and late. We apply this approach to the Boise Hydrogeophysical Research Site and find that the equivalent property spatial averages decrease with horizontal distance from the pumping well and appear to stabilize at sufficiently large distances, in line with existing theory for K_{eq}. The squared coefficient of variation shows similar behavior, with values indicating a weakly heterogeneous aquifer. Furthermore, estimated values for K_{eq}, $S_{s,eq}$, and $S_{y,eq}$ are in agreement with literature values for the site.

1. Introduction

Dealing with fundamental groundwater challenges such as contamination, depletion, and salinity requires advanced modeling and aquifer characterization. Pumping tests have been used for estimating aquifer hydraulic properties for over a century. It is well known that for many groundwater applications, incorporating heterogeneity into flow models is paramount for accurate predictions. For this reason, tomographic tests are used to characterize the spatial distribution of hydraulic properties. In these tests, pumping is conducted at various wells and at specific intervals (isolated using packers), while pressure is monitored at many locations (i.e., intervals) in surrounding observation wells. Analysis of the large amounts of data accumulated in these tests to characterize aquifer heterogeneity has been the subject of a considerable body of literature (reviewed below). In this work, we present and implement a new approach, based on calculating spatially distributed equivalent properties from continuous pumping tomography tests and characterizing their statistical properties.

The simplest approach to aquifer property estimation assumes that the aquifer is homogeneous with constant properties: hydraulic conductivity K, specific storage S_s, and specific yield S_y. However, this is often not an accurate description of the aquifer and leads to significant modeling errors. For heterogeneous aquifers, it is common to assume that K (and sometimes also S_s) are random space functions of a given distribution and to seek a "most likely" solution in a stochastic framework. A large body of literature has adopted this type of approach (e.g., Kitanidis & Vomvoris, 1983; Neuman & Yakowitz, 1979; Yustres et al., 2012) and a summary is presented in Carrera et al. (2005). Applying this approach to analysis of tomography-type pumping tests is a procedure often referred to as hydraulic tomography (HT) in the literature, though strictly speaking, any test with multiple pumping and measurement locations is considered HT.

Conventional HT analysis entails solving an inverse problem on a discretized aquifer domain with many thousands of unknown variables. Early HT inverse methods (e.g., Carrera and Neuman, 1986; Gottlieb and Dietrich, 1995; Yeh et al., 1996) has evolved to more robust and validated algorithms (e.g., Cardiff and Barrash, 2011; Cardiff et al., 2012; Hochstetler et al., 2016; Zha et al., 2018); a thorough review of HT literature and field studies is presented in the work of Cardiff and Barrash (2011). There are various problematic aspects of the HT inverse methods, the first and foremost of which is that the problem is ill posed (Bohling & Butler, 2010). Furthermore, to achieve accurate estimation many data measurements are required, which are often not available. Moreover, while the preferred inversion method is stochastic and can be used for uncertainty analysis, the emphasis in previous literature is usually on a single "most likely" result, for example, a spatial map of hydraulic conductivity, and these maps are often misinterpreted as a deterministic result. The method is also extremely demanding in terms of computational cost. Finally, HT results are also difficult to verify in field experiments since pointwise measurements, or independent tests for comparison, are usually scarce.

All the above literature, including HT and earlier estimation methods, are based on discretization of the aquifer domain and estimating the parameters in those discrete zones using a numerical solution for the flow problem. Furthermore, most of the literature focuses on development of different methods of this nature and validation using synthetic examples. Only a limited number of studies include application to high resolution 3D field experiments (Berg & Illman, 2011; Cardiff, Barrash, & Kitanidis, 2013; Cardiff et al., 2012; Hochstetler et al., 2016; Tiedeman & Barrash, 2020). In addition, the estimated hydraulic property values (primarily K) are often used in applications (e.g., contaminant transport) considering a large aquifer volume extending past the one investigated by the HT and therefore one has to extrapolate them in space. To achieve this goal, the stochastic approach assumes that K is a stationary random field whose statistical properties, such as probability density function and two point covariance, are derived from the analysis of the HT determined values. Then, realizations of K values can be spatially generated using standard algorithms such as sequential Gaussian simulation. In the spirit of previous work, the procedure adopted here aims at deriving the statistical moments of K, S_s, and S_y directly from those of the measured head values (H), circumventing the pointwise identification implied by HT.

The first goal of this work is to present a new approach for analysis of a continuous pumping tomography field test based on statistical characterization of the hydraulic equivalent properties (K_{eq}, $S_{s,eq}$, and $S_{y,eq}$) associated with the measured H. This entails determining an equivalent property pertaining to each measurement location by fitting a semianalytical solution of a homogeneous model to the measured head time signal. Then, averaging in space and over different tests is conducted to arrive at statistical parameters of the aquifer (first two statistical moments of equivalent properties), that is, the variation of the mean equivalent properties and their coefficients of variation with distance from the pumping well. The second goal is to show feasibility of the new method by applying it to a field case, that is, a tomographic pumping test at the Boise Hydrogeophysical Research Site (BHRS). The method is validated by comparing the results to previous literature values obtain from the many different tests that have been conducted at the site. Finally, the analysis of the field data leads to some interesting findings regarding the statistical behavior of the equivalent properties, namely that their mean decreases with distance from the pumping well and appears to converge to the effective value at a distance.

The method presented in this work is based on ideas first discussed for steady flow in Indelman et al. (1996), Indelman (2001), more recently in Cheng et al. (2019, 2020), and applied to a synthetic case in Bellin et al. (2020). The latter-most work proposed a procedure for estimating the statistical moments of K, S_s, and S_y from the moments of the equivalent properties considering steady source flow in an unbounded aquifer. This is in principle applicable to the results of this work, though we consider the more complex case of a continuous source and bounded (phreatic) aquifer. The general procedure involves the following steps: (a) calculating the distribution of the statistical moments of K_{eq} as a function of distance from the pumping source by analysis of the measured H data; (b) deriving an approximate theoretical solution for source flow in a heterogeneous medium, rendering the moments of K_{eq} as functions of those of K; and (c) the latter are identified by a best fit of the moments of the measured and theoretical K_{eq}. The procedure was illustrated by Bellin et al. (2020) for a synthetic case. Here, the first step of the method is further developed and implemented for the first time on field data in order to characterize the BHRS.

In view of the complexity of the problem the present study is addressing solely the first step discussed above, that is, the statistical analysis of hydraulic equivalent properties of the BHRS. This step already needs development of innovative methodologies and a substantial effort, as shown in Section 4. The subsequent two steps of identification of the moments of the point values is the objective of future studies. Nevertheless, even the first step of estimation equivalent properties provides valuable information for practitioners, such as the overall effective properties and insight on the heterogeneity of the aquifer. Ultimately, the results of this work can hopefully serve for characterization of heterogeneous aquifers toward application to prediction of flow and transport under natural gradient or radial well flow conditions.

The novelty of this work is first and foremost in the development of the approach for characterizing heterogeneity, as detailed above. We apply this approach for the first time considering continuous pumping (as opposed to steady state), unconfined aquifers, multiple partially penetrating pumping and observation wells, and accounting for the random spatially varying S_s and S_y (in addition to K). The second novelty is the application considering a real field case, which is the ultimate feasibility test. The third novelty is the method developed in this work for estimating equivalent properties by separation of the head time signal to two time periods, as described in detail in Section 4. This method allows an additional validation of the results for K_{eq}, as it is calculated independently by each of the time periods. The fourth novelty is the estimation of the coefficient of variation of S_s and S_y in a field study, which to the best of our knowledge has not been previously published.

The investigated BHRS is a research wellfield with 18 fully screened wells through a shallow unconfined aquifer consisting of approximately 16 m saturated thickness of coarse fluvial sediments. The aquifer has well-documented hierarchical heterogeneity of layers with distributed lenses of variable facies recognized from the following: core and borehole logs (e.g., Barrash & Cardiff, 2013; Barrash & Clemo, 2002; Barrash & Reboulet, 2004; Mwenifumbo et al., 2009), cross-hole geophysics (e.g., Binley et al., 2016; Clement & Barrash, 2006; Dafflon & Barrash, 2012; Tronicke et al., 2004), and hydrologic testing (e.g., Barrash et al., 2006; Cardiff & Barrash, 2011; Dafflon, Irving, & Barrash, 2011; Malama et al., 2011; Straface et al., 2011). In particular, high-resolution high-quality K profiles in wells from slug tests (Barrash & Cardiff, 2013; Cardiff et al., 2011) as well as HT analyses (Cardiff et al., 2012; Cardiff, Barrash, & Kitanidis, 2013) were conducted at the site. The many previous investigations of the BHRS will serve us in validating the new approach presented here. For more details on the BHRS and the pumping tests carried out to obtain the data for this work, please refer to Section 3.

Estimating statistical parameters such as mean and variance of equivalent properties, which is the aim of the present study, is a more modest goal than determining the pointwise properties as in HT methods. Nevertheless, there are a number of important advantages. First, the problem is well posed, requiring only two parameters to be calculated simultaneously in an inverse procedure. Second, the procedure is robust, reliable, and efficient, making use of simple semianalytical solutions rather than numerical simulations. Third, previous studies have derived and discussed derivation of statistical properties of aquifers in analytical and semianalytical models considering uniform flow (e.g., Dagan, 1989) and well-induced flow (e.g., Indelman et al., 1996). The results of this work can be used for comparison with such theoretical literature, to validate it and draw insight on the underlying physics. Finally, the current method can be used to validate and support the more detailed (yet more laborious) HT methods. We note that assuming the aquifer properties are stationary random variables, the estimated parameters are applicable to a relatively large region, extending outside the limited area of the experimental site.

The concept of a property similar to equivalent hydraulic conductivity was discussed as far back as Matheron (1967), who considered steady flow between two fully penetrating cylinders of constant head and defined K_{eq} as the K of a homogeneous medium leading to the same discharge as the actual heterogeneous medium for the given head drop. Indelman et al. (1996) studied K_{eq} pertaining to steady flow from a fully penetrating well in a confined heterogeneous aquifer and found that its mean varies with distance from the well, that is, from the arithmetic mean of K near the well to the uniform flow effective conductivity (K_{efu}) far from the well. A similar variation of K_{eq} was found in Wu et al. (2005), yet as a function of time rather than distance, for numerical simulations of radial flow to a well in a 2D aquifer. Cheng et al. (2019) calculated K_{eq} for oscillatory pumping based on their derived mean head amplitude by a first order approximation in variance of log conductivity. Bellin et al. (2020) derived dependence of K_{eq} on K statistics and distance from a source for steady flow and compared with calculated K_{eq} from a synthetic case. All the above literature is focused on theory, with some limited use of real pumping test data from the BHRS in Cheng et al. (2019). Only the work of Rabinovich et al. (2015) consists of a K_{eq} investigation using data from a field oscillatory pumping test, however, the current method is not applied, as only a single K_{eq} value is assumed for the entire aquifer, without a statistical analysis of spatial variation.

The structure of this paper is as follows. In Section 3, we describe the BHRS and the pumping tests carried out to generate the data used in this work. In Section 4, we present the homogeneous solutions used in this work and our approach for calculating equivalent properties by implementation of these solutions. Section 5 details the analysis of the pumping test data and the calculation of the statistical moments of the equivalent properties. Finally, Section 6 summarizes the results and the main conclusion.

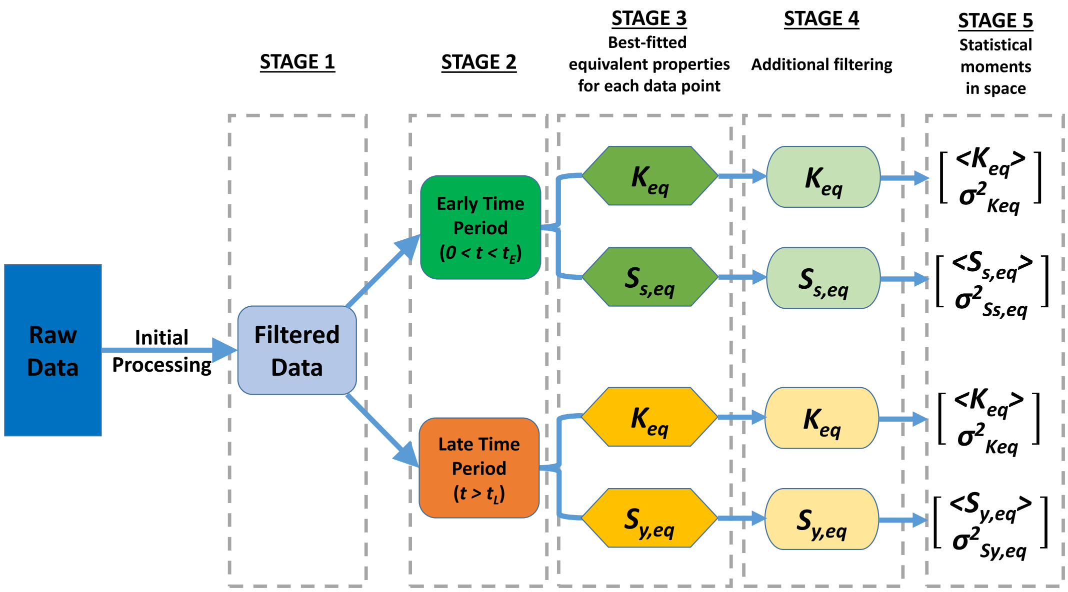

Figure 1. Flow chart of the new method detailing the stages of calculating statistical moments of aquifer equivalent properties.

2. Method

In this section, we will present the method for calculation of the first two statistical moments of the aquifer equivalent properties. Keep in mind that the method is described here only in general terms, while many additional details are provided in the following sections.

We assume that a tomographic constant rate pumping test has been carried out in a given aquifer. For simplicity, the pumping location is assumed to be at a point in space, though in reality this could be the center of the pumping well segment. Considering a Cartesian coordinate system, the pumping source is assumed to be located at $x = y = 0$ and $z = Z$ (note that $Z < 0$), where $z = 0$ is the top of the aquifer (e.g., the initial water table). We also use a cylindrical coordinate system appropriate for the axisymmetric nature of the problem, with $R = \left(x^2 + y^2\right)^{1/2}$, $\varphi = \tan^{-1}(y/x)$, z and the pumping location is therefore at $R = 0$, $z = Z$. The pressure head associated with a pumping at source $z = Z$, at an observation point (R, φ, z) is denoted as $H_Z(R, \varphi, z, t)$. The tomographic test data consists of many head time series $H(t)$ at the various observation points (R, φ, z) and for various tests conducted at different pumping locations Z.

Figure 1 gives a general description of the procedure in the form of a flow chart. The first stage of the method consists of smoothing the head data signals $H(t)$ by fitting them with a smooth function and filtering out any $H(t)$ curves that appear nonphysical, for example, those with a large error in comparison to the fitted analytical solution (see Section 3.3 for more details). Then, the $H(t)$ signal is divided into two time periods: an early period, in which the effect of water table drainage can be neglected and a late period, in which the aquifer storativity can be neglected. This is stage 2 in Figure 1 and described in detail in Section 4.2.

Stage 3 of the method involves estimating the equivalent properties by matching a homogeneous model to the head data $H(t)$, separately for each time period. This leads to values of K_{eq} and $S_{s,eq}$ for the early time period and K_{eq} and $S_{y,eq}$ for the late time period (stage 3 in Figure 1). Therefore, for each "data point" with an observation location of (R, φ, z) and pumping location Z, the three equivalent properties are obtained. Section 4.3 provides more details on implementation of this stage. Next, in stage 4, an additional filtering is applied by removing data points in which the estimated equivalent properties have unreasonable values, that is, very far from the mean. The final stage, that is, stage 5, consists of calculating the average and variance (or coefficient of variation) of each equivalent property. Here, we only average overall the observation point locations within the same layer of given $|z - Z|$ value. For example, considering $|z - Z| = 0$ (i.e., $z = Z$), we obtain equivalent property mean and variance as a function of R. We note that K_{eq} mean and variance are calculated twice (once for early time and also for late

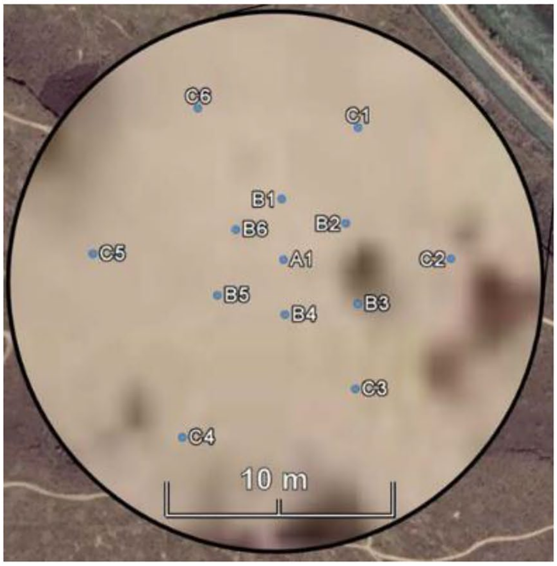

(a)

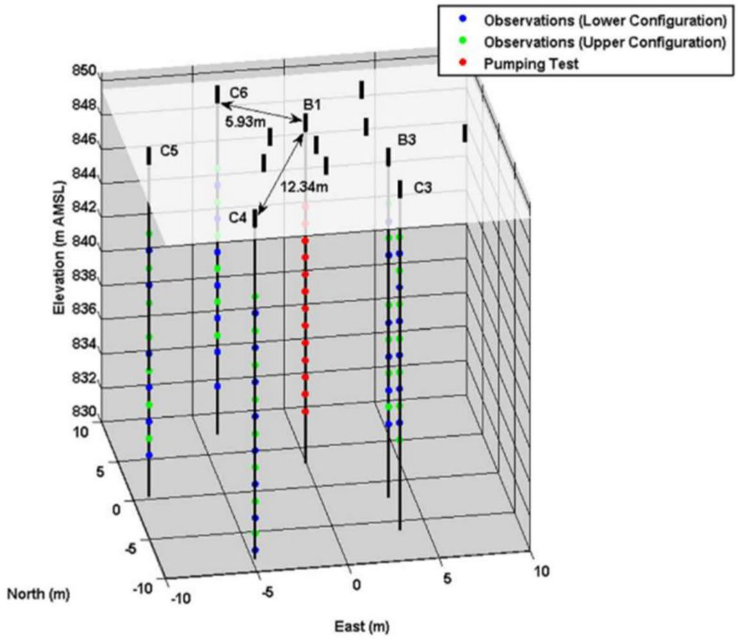

(b)

Figure 2. The Boise Hydrogeophysical Research Site—well layout (taken from Cardiff, Barrash, & Kitanidis, 2013). (a) The well distribution map from an aerial view. (b) The experimental setup for the case of pumping at B1 and five observation wells. Various measurement and pumping vertical locations are indicated.

time) and therefore the K_{eq} results can be validated by comparing the two values. This is a valuable feature of the method.

3. Site Description, Experimental Setup, and Data

3.1. BHRS

The BHRS is a research wellfield located in proximity to the Boise River, about 15-km upstream from downtown Boise, ID, USA. Eighteen wells of approximately 10 cm diameter were drilled on site using a core-drill-drive method and screening. The wells are arranged in three rings around a central well, where the 13 wells of the two inner rings are depicted in Figure 2a, consisting of the outer ring (wells C1–C6) and inner ring (wells B1–B6), surrounding the central well A1. The fluvial aquifer is composed of mostly coarse cobble, gravel, and sand sediments (Barrash et al., 2006), confined below by a clay layer and unconfined from above. The thickness of the aquifer is 15.8 m on average, varying slightly due to the presence of a basalt zone immediately above the clay confining layer, which was observed in some of the wells.

Heterogeneity of the aquifer was characterized through analysis of stratigraphy via neutron porosity logs (Barrash & Clemo, 2002) and core analysis (Barrash & Reboulet, 2004), leading to identification of five distinct geological units on site. These were verified by geophysical surveys using ground-penetrating radar (GPR) (Clement & Barrash, 2006; Clement & Knoll, 2006; Clement et al., 2006; Dafflon, Irving, & Barrash, 2011; Ernst et al., 2007; Irving et al., 2007), seismic (Moret et al., 2004, 2006), induced polarization (Binley et al., 2016), and capacitive conductivity (Mwenifumbo et al., 2009) methods. Investigations of hydraulic conductivity variability throughout the site have been carried out with a variety of methods, including analytical curve fitting of individual fully penetrating pumping tests (Barrash et al., 2006), joint analysis of tracer test breakthrough curves (Dafflon, Barrash, et al., 2011), tomographic analyses of fully penetrating pumping tests (Cardiff et al., 2009; Straface et al., 2011), analytical curve fitting of evapotranspiration responses in wells (Malama & Johnson, 2010), analytical curve fitting of individual partially penetrating slug test responses (Barrash & Cardiff, 2013; Cardiff et al., 2011; Malama et al., 2011), oscillatory HT (Cardiff et al., 2020; Rabinovich et al., 2015), and imaging from 3D transient HT (Cardiff et al., 2012; Cardiff, Barrash, & Kitanidis, 2013). These methods reported consistent estimates of hydraulic conductivity with overall average values of 1.5–9 × 10^{-4} m/s. The higher values are estimated in slug pumping tests which are known to be large at the BHRS in comparison to other field tests (Cardiff et al., 2012). Therefore, we refer to a reduced average value for literature K (excluding slug tests) of 3 × 10^{-4} m/s.

Estimated S_s, S_y, and variances of hydraulic properties in the BHRS are hardly discussed in previous literature. Variance of $\ln K$, denoted by $\sigma^2_{\ln K}$, is reported to have values of 0.36–0.92 in Cardiff, Bakhos, et al. (2013) and the overall variance is considered to be 0.49 (Barrash & Cardiff, 2013). Estimation of S_s and S_y was found only in Barrash et al. (2006); Rabinovich et al. (2015) with average overall values of 3.8 × 10^{-5} and 0.028, respectively (Barrash et al., 2006). The above literature values are presented in an organized manner in Table 2. Estimated values of variances of $\ln S_s$ and $\ln S_y$ ($\sigma^2_{\ln S_s}$, $\sigma^2_{\ln S_y}$) have not yet been reported for the BHRS.

3.2. Field Test

We consider data accumulated during a field test conducted in the summer of 2011 at the BHRS. A series of partially penetrating pumping tests were carried out at successive 1 m intervals in three pumping wells: A1, B1, and C1 with pressure responses recorded in seven surrounding wells: B3, C1, C2, C3, C4, C5, and C6. The test setup for an example case in which pumping is carried out at well B1 and observations in wells B3, C3, C4, C5, and C6 is illustrated in Figure 2b. Each observation well was equipped with a packer-and-port string consisting of seven 1 m open intervals separated by a 1 m inflatable packer above and below. This allowed for independent measurements of head as a function of time $H(t)$ at successive 1 m intervals in each observation well. Furthermore, the strings allowed for tests in two different configurations, that is, "upper" and "lower" (see Figure 2b), therefore doubling the number of measurement data points accumulated in each observation well. Altogether, 2,472 measurements of $H(t)$, corresponding to different observation and pumping locations, were available for data analysis.

Pumping flow rate and duration varied between the different tests, with rates in the range 25.35–60.68 L/min and duration between 13 and 15 min. The test duration was chosen to be short enough for efficiency, considering the numerous pumping tests conducted, yet long enough to reach "late time" behavior of the unconfined aquifer (see Sections 4.2.2 and 4.3). Head changes were monitored in wells C4, C5, and C6 using small-diameter fiber-optic pressure transducers (FISO model FOP-MIV-NS-369D) with errors that were verified to be as small as 1 mm water pressure. The remainder of the pressure change observations was recorded using standard strain-gage pressure transducers (Druck model POCR 1930-8388). For additional details regarding the pumping tests, we refer readers to Cardiff, Barrash, and Kitanidis (2013); however, we note that they only include pumping from well B1. The additional data used in this work from pumping wells A1 and C1 did not appear in previous publications.

3.3. Initial Data Treatment

As a first step in data processing, we smoothed the $H(t)$ curves by fitting them with a MATLAB Lowess Smoothing function, thus removing any unwanted noise from the signal. We found that this procedure facilitated the estimation of equivalent properties by best fitting without affecting the results. Of the 2,281 total $H(t)$ data curves, we eliminate curves which are suspected to be nonphysical by implementing two constraints. First, we remove curves that during the equivalent property calculation stage (see description in next section) have a large deviation from the semianalytical model fitting. The error between measured and model $H(t)$ is expressed by the objective function described in Section 4.3. Data sets are eliminated if the error calculated by Equation 7 is larger than 5%, indicating deviation of $H(t)$ from the semianalytical model fit. The second constraint involves removing curves that lead to outlier values of estimated properties, that is, values which are very far from the overall mean (e.g., more than two standard deviations from the mean). This constraint also eliminates the cases in which a minimum of the objective function was not found. We further discuss the number of removed curves and their impact in Section 5.

4. Calculating Equivalent Properties in a Tomographic Test

The calculation of equivalent properties at various observation points in a tomographic pumping test is based on the solution of the flow equations for a homogeneous medium with the boundary and initial conditions pertinent to the test. The basic solution considered here is that of a continuous source in an unconfined

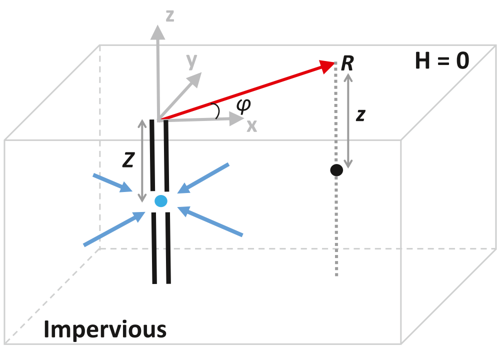

Figure 3. Schematic illustration of the pumping test model with pumping source located at $(0, 0, Z)$ and measurement point at (R, φ, z).

aquifer. Although approximate solutions for such unsteady flows have been derived along time ago, it is useful to implement simplified solutions for the analysis due to the large number of observation points associated with tomographic tests. Such an approach of using simplified solutions is advanced here for the first time (the advantages are detailed at the end of this section) and it is used in the next section for the analysis of the BHRS test measurements.

We use the notation of Section 2 and Figure 3, with the origin of the axes located at the initial water table, immediately above the pumping segment. A point source is used here to represent the pumping well (line source) as it is was found to be sufficiently accurate (discussed further in the beginning of Section 4.3). The equivalent properties at an observation point, can be generally defined as those of a homogeneous medium, under the same boundary conditions and source term, which lead to approximately the same head response $H(t)$ as the one prevailing in the heterogeneous medium. The following is a description of the classical homogeneous model, which will be used for calculating equivalent properties. We note that the models derived below assume homogeneous and isotropic aquifers. The latter simplification will allow the use of a theoretical solution for equivalent properties (second step mentioned in the Introduction, intended to be carried out in future work) for the same conditions toward fitting between the measured and theoretical statistical moments (third step mentioned in the Introduction). The possible use of flow solutions for a homogeneous and anisotropic medium is deferred to future studies.

4.1. Source Flow in a Homogeneous Aquifer

For an unconfined aquifer of homogeneous properties K, S_s, and S_y, a water table elevation given by some function $z = -\zeta(R, \varphi, t)$, and a pumping point source of discharge $Q > 0$ for $t > 0$, the governing equation for the head $H(x, y, z, t)$ is given as follows:

$$S_s \frac{\partial H}{\partial t} - K\,\nabla^2 H = -Q\delta(x)\delta(y)\delta(z - Z) \qquad (-D < z < -\zeta,\;\; t > 0), \tag{1}$$

where δ is the Dirac operator and D is aquifer thickness. The aquifer is assumed to be isotropic and infinite in the horizontal direction with the following boundary conditions, pertaining to an unconfined aquifer of constant S_y:

$$S_y \frac{\partial H}{\partial t} + K\frac{\partial H}{\partial z} - K\nabla H \cdot \nabla H = 0 \qquad (z = -\zeta), \tag{2a}$$

$$\frac{\partial H}{\partial z} = 0 \qquad (z = -D). \tag{2b}$$

The initial condition is $H(x, y, z, 0) = 0$ (prior to the onset of the pumping) and the boundary condition in the horizontal direction is $H(R \to \infty, z, t) = 0$.

Due to the nonlinearity of the free surface condition given by Equation 2a, an approximation was adopted in the literature to allow for simplified solutions. Following Dagan (1967) and Neuman (1974) (see also Yeh et al. (2010)), the condition is linearized by neglecting the quadratic term and assuming that the water table drop is small compared to the aquifer thickness, that is, $\zeta/D \ll 1$. Subsequently, the flow domain becomes $-D < z < 0$ in Equations 1 and 2a is replaced by the following equation:

$$S_y \frac{\partial H}{\partial t} + K\frac{\partial H}{\partial z} = 0 \qquad (z = 0), \tag{3}$$

where $\zeta(x, y, t) = H(x, y, 0, t)$.

A semianalytical solution for $H(x, y, z, t)$, as described by the system above, is derived in Neuman (1974) (coined as the delayed yield solution). The solution is illustrated in Neuman (1974, Figures 4–6) for the drawdown $s(t) = -H(t)$, considering a given choice of dimensionless parameter values and coordinates. It requires numerical

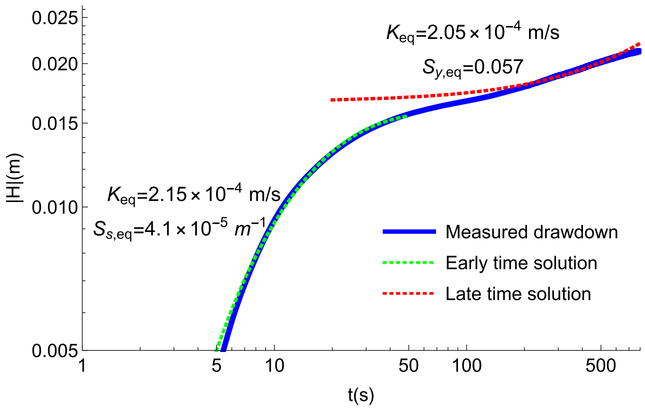

Figure 4. Example of measured drawdown data set $|H(t)|$ at location ($R = 9.5$ m, $\varphi = 0.7$, $z = 7.9$ m) for a test with pumping interval at $Z = 7.9$ m in well A1. Homogeneous solutions of early time (Equation 5) and late time (Equation 6) are fitted to the data curve.

inversion of the Laplace transform of the drawdown and commercial codes are available for its implementation. However, unlike in standard pumping tests, in the present work it has to be applied hundreds of times for the numerous observation points. Furthermore, it implies the simultaneous identification of the optimal values of the three parameters K_{eq}, $S_{s,eq}$, $S_{y,eq}$ by a best fit of the computed and observed heads. To reduce the computational effort in the present work, we prefer to implement two simpler solutions for calculation of equivalent properties and this has some advantages in the inverse procedure, as will be explained in the following. We note that due to linearity of the system of Equations 1, 2b, and 3, the solutions presented below can be easily extended to a pumping well of finite length by integration over Z and an observation well of finite length by integration over z.

4.2. Simplified Solutions

Analyzing the solution of Neuman (1974), we find that $H(t)$ at any given point in space can be divided into three time periods as follows.

4.2.1. Early Time Period ($0 < t < t_E$)

At sufficiently early times (denoted $t < t_E$, where t_E is the endpoint of the early time period), the impact of the water table is negligible and water is drawn from the bulk of the aquifer due to the elastic response solely. Indeed, as shown in Neuman (1974) (Figure 2) or in Figure 4 here, the solution of Dagan (1967) (derived for unconfined nonelastic formations) tends to a constant head at early times ($t < t_E$), indicating the negligible contribution of the specific yield. Under this assumption, the water table is practically flat and the boundary condition at $z = 0$ is now $H = 0$, replacing Equation 2a in the system of governing equations, while S_y is immaterial. A solution was provided by Carslaw and Jaeger (1959, Equation 10.4.2) for the similar problem of heat flow. For an unbounded domain it is given by the following equation:

$$H_\infty(r,t) = -\frac{Q}{4\pi K r}\operatorname{erfc}\left[\frac{r}{2}\left(\frac{S_s}{tK}\right)^{1/2}\right], \tag{4}$$

where $r = \left[R^2 + (z - Z)^2\right]^{1/2}$ is the distance from the source and erfc is the complementary error function. To account for the boundary conditions at $z = 0$ and $z = -D$, the method of images (see Carslaw and Jaeger (1959, Section 10.10) for a similar problem) is implemented and the solution is given by the following equation:

$$\begin{gathered} H_Z(R,z,t) = \sum_{m=-M}^{M}\left[H_\infty(r_m,t) - H_\infty(r_m^*,t)\right], \\ r_m = \left\{R^2 + \left(2mD + \left[z - (-1)^m Z\right]\right)^2\right\}^{1/2}, r_m^* = \left\{R^2 + \left(2mD + \left[z - (-1)^{m-1} Z\right]\right)^2\right\}^{1/2}. \end{gathered} \tag{5}$$

While Equation 5 is exact only for $M \to \infty$, it is emphasized that it often converges quickly, for example, for the data pertinent to the BHRS test, retaining eight terms ($M = 4$) is sufficient to ensure accuracy for all measurement points at any $t < t_E$ ($t_E \approx 50$ s for BHRS). Furthermore, Equation 5 provides an accurate approximation of the full solution of Neuman (1974) at sufficiently early times and the accuracy of the approximation will also be discussed in Section 4.3 regarding the BHRS data (see Figure 4).

4.2.2. Late Time Period ($t > t_L$)

At sufficiently late times (denoted $t > t_L$, where t_L is the start point of the late time period), the water table drainage dominates in comparison to elastic storage if $S_y \gg S_s D$, which is generally the case (for the BHRS test $S_s D/S_y \approx 10^{-3}$). Then, the first term in Equation 1 can be neglected and S_s becomes immaterial while S_y is practically constant (instantaneous drainage). This case was treated by Dagan (1966, Equation 31) (following the works of

Theis (1935) and Hantush (1961), e.g., see Schwartz and Zhang (2003)), who derived a semianalytical solution given by the following equation:

$$H_Z(R,z,t) = -\frac{Q}{4\pi K}\left\{\frac{1}{\left[R^2+(z-Z)^2\right]^{1/2}} + \frac{1}{\left[R^2+(z+Z)^2\right]^{1/2}} - 2\int_0^\infty\left[\frac{e^{-\lambda t(K/S_y)\tanh\lambda D}\cosh[\lambda(z+D)]\cosh[\lambda(Z+D)]}{\sinh(\lambda D)\cosh(\lambda D)} - \frac{e^{-\lambda D}\cosh(\lambda z)\cosh(\lambda Z)}{\sinh(\lambda D)}\right] J_0(\lambda R)d\lambda.\right. \tag{6}$$

Equation 6 approximates accurately the Neuman (1974) solution at late times, as seen in Neuman (1974, Figure 2) for the curve denoted by "Dagan's solution." This will be further discussed in Section 4.3 and shown to be the case also for the BHRS data for $t_L \approx 200$ s (see Figure 4).

4.2.3. Intermediate Time Period ($t_E < t < t_L$)

In this time period there is a transition between the two previous regimes of early and late times. Both elastic storage and water table yield have a nonnegligible contribution and therefore the full solution of Neuman (1974) is appropriate. However, even this solution may not be applicable (Mao et al., 2011), as it assumes instantaneous drainage, while in fact S_y is not constant and should be modeled as time dependent. To overcome this issue, it was proposed to model the flow in the unsaturated zone above $z = 0$, circumventing the use of S_y. Early works of Kroszynski (1975) and Kroszynski and Dagan (1975) have advanced an approximate model which was adopted by Tartakovsky and Neuman (2007). They generalized the Neuman (1974) solution and used, in addition to S_s and S_y, the parameter κ of Kroszynski and Dagan (1975), where κ^{-1} is proportional to the thickness of the unsaturated zone under equilibrium. The complex solution was used by Tartakovsky and Neuman (2007) to illustrate the impact of the magnitude of the parameter κD on the solution, for a particular choice of other parameters. We note that the late time period solution is also affected by time dependent S_y; however, in Tartakovsky and Neuman (2007, Figures 2–6), it is seen that for $\kappa D \geq 10$ and $t > t_L$, the instantaneous drainage solution is quite accurate and the approximation of Equation 6 is valid. This is believed to be the case for the BHRS (as well as for most aquifers) as the aquifer thickness is $D = 15.8$ m and the unsaturated zone is expected to be less than one m thick for typical aquifers (Kroszynski & Dagan, 1975).

4.3. Application to the Head Signals in the BHRS Test

A typical pressure head signal (i.e., time-drawdown) from the BHRS data is presented in Figure 4. The plotted head as a function of time $H_Z(R, z, \varphi, t)$ is measured at an observation interval located at $R = 9.5$ m, $z/D = -0.5$, and $\varphi = 0.7$, induced by pumping at well A1 with interval elevation of $Z/D = -0.5$. It can be seen that the $H(t)$ curve has the typical sigmoid shape of the Neuman (1974, Figure 2) solution. Furthermore, along the lines of the above decomposition, we have best fitted the two simplified solutions of Equations 5 and 6 corresponding to the early and late time periods, respectively. First, it was checked that the solution for a pumping segment of 1 m could be accurately replaced by that of a point source at its center (Z). We found that even for the closest measurement location of $R = 4.2$ m, a point source solution is approximately the same as the corresponding 1 m line source solution. Therefore, the point source solution was used hereafter in the analysis. We note that the onset of pumping was not taken to be at $t = 0$ for the simplified solutions but rather the time corresponding to the experimental data, seen to be $t \approx 5$ s in Figure 4. This time shift accounts for effects like the transient in the establishment of the pumped discharge or the well-bore volume. It is emphasized that a uniform shift of 5 s was applied to the solutions, for accurate fitting of the data.

The data in Figure 4 and all other $H(t)$ curves in this work were fitted by minimizing the objective function given by the following equation:

$$Obj = \frac{\langle |H_{test}(t_i) - H_{model}(t_i)|\rangle_{t_i}}{H_{test}(t_{ref})}, \tag{7}$$

where H_{test} is the measured head from the pumping test data and H_{model} is the semianalytical solution of Equation 5 or Equation 6. The time t_i is the i'th member in the series of discrete time measurements, the brackets indicate averaging overall times and t_{ref} is the reference time of the series, which was taken to be t_E for the early time analyses and $T_{end} = 600$ s for the late time period analysis. The parameters K_{eq}, $S_{s,eq}$, and $S_{y,eq}$ were obtained by finding the minimum of Equation 7 using the Wolfram Mathematica "NMinimize" function.

It is observed in Figure 4 that indeed a very good fit could be attained with calibrated values of $K_{eq} = 2.15 \times 10^{-4}$ m/s, $S_{s,eq} = 4.1 \times 10^{-5}$ 1/m for the early time period and $K_{eq} = 2.05 \times 10^{-4}$ m/s, $S_{y,eq} = 0.06$ for the late period. Furthermore, t_E was found to be around 50 s, whereas $t_L \approx 200$ s for all signals and except for a few outliers the fit by Equations 5 and 6 was very accurate. Nevertheless, the fit consists of matching a homogeneous aquifer solution to field data of a heterogeneous aquifer, and therefore some mismatch is expected, as seen in the plot. Furthermore, the early time and late time fittings were done completely independent of each other and yet the two obtained K_{eq} values are very close to one another (~5% difference in the plotted example), showing consistency of the simplified solution approach. Thus, the set of time dependent signals could be replaced by a table with the values of the three parameters K_{eq}, $S_{s,eq}$, and $S_{y,eq}$, being understood that they represent the underlying simple solutions of Equations 5 and 6. These are the values to be used in Section 5 toward the statistical analysis of the equivalent properties.

The replacement of the Neuman (1974) complex solution by the simplified early and late ones of Equations 5 and 6 has some definite advantages: (a) it simplifies considerably the repetitive best fit calculations for the numerous signals, thus decreasing the computational cost; (b) it separates the derivation of $S_{s,eq}$ and $S_{y,eq}$, requiring only two-variable optimization rather than three, and (c) it avoids the use of the intermediate period in the Neuman (1974) solution, which was seen to be the most error prone due to the assumption of instantaneous drainage, that is, constant $S_{y,eq}$.

5. Statistical Analysis of the Equivalent Properties

5.1. General

The basic data of the BHRS test consists of a collection of head signals $H_Z(R, \varphi, z, t)$ (Section 3), where we note again that R, φ are the planar coordinates of a pressure transducer at the vertical location z, relative to a pumping source at $R = 0$, $z = Z$ (Figures 2–4). By the procedure described in Section 4, the head time signals are encapsulated by the two numbers K_{eq}, $S_{s,eq}$ at early times (roughly $t < 50$ s) and K_{eq}, $S_{y,eq}$ at late times (roughly $t > 200$ s, see Figure 4), which are functions of R, φ, Z, z. In the spirit of the theoretical studies of Indelman et al. (1996) and Bellin et al. (2020) for steady state (who dealt only with K_{eq}), we assume that the spatial variability of K_{eq}, $S_{s,eq}$, $S_{y,eq}$ stems from that of the underlying local properties K, S_s, S_y. Furthermore, in line with the common approach of modeling heterogeneity (e.g., Dagan, 1989), it was assumed in the aforementioned studies that $\ln K$ can be modeled as a multi-Gaussian stationary field, completely characterized by the constant mean $\langle \ln K \rangle = \ln K_G$ (where K_G is the geometric mean), the variance $\sigma^2_{\ln K}$ and the horizontal I and vertical I_v integral scales of the axisymmetric two-point covariance (i.e., $I = \int \rho \mathrm{dR}$, where ρ is the autocorrelation function of $\ln K$). Thus, for a line source representing a fully penetrating well (Indelman et al., 1996) and a point source (Bellin et al., 2020), K_{eq} was shown to be a nonstationary random field, with $\langle K_{eq} \rangle$ and $\sigma^2_{K_{eq}}$ functions of distance R from the source. Furthermore, $\langle K_{eq} \rangle$ decreased between $\langle K \rangle$ for $R \ll I$ and K_{efu} for $R > I$, where K_{efu} is the effective conductivity in uniform flow. The latter is a fundamental property of the heterogeneous medium as it relates the mean specific discharge to the mean head gradient under conditions of natural gradient flow.

A vast literature was devoted to the relationship between K_{efu} and the statistical moments of K (for a recent article see for instance Zarlenga et al. (2018)). The two limits are easy to grasp intuitively: near the source, where the head gradient is large, and for $R \ll I$, the medium behaves like a homogeneous one of the local K ($K_{eq} = K$); in contrast, at large distance the head gradient is slowly varying and the flow is essentially uniform. The main aim of common pumping tests is to identify K_{efu}, prevailing at sufficiently large distances from the pumping well, where the mean flow becomes practically horizontal, even for partially penetrating wells.

In order to simplify the statistical analysis of the BHRS, while minimizing the effects of boundaries and in accordance with the isotropy assumption, we consider signals for which $z \cong Z$, that is, the pumping interval center and the observation point are in the same horizontal plane (Figure 5). For the available discrete values of Z and z (Figure 2b), there are few observation points for which $z = Z$ exactly, therefore we selected for any given source at Z the observation point within $|z - Z| < 1$ m, that is, z is close to Z within a meter. Figure 5 illustrates the band of 2 m width around each pumping source in which observation points are included in the analysis, demonstrated

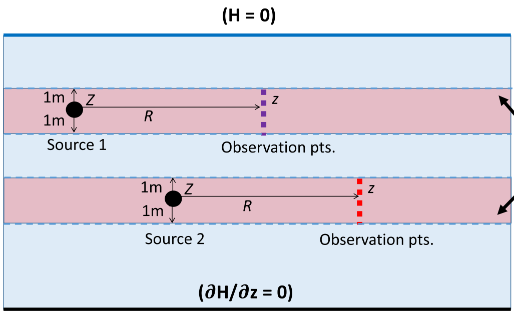

Figure 5. Illustration of measurement data included in the $|z - Z| < 1$ m analysis. Two pumping sources are depicted and a 2-m band in which observation data is included in the equivalent property analysis.

for two sources. Thus, the data set used in order to analyze the statistical properties of the hydraulic properties are now K_{eq}, $S_{s,eq}$, $S_{y,eq}$ functions of R, φ, Z (for $|z - Z| < 1$ m). We note that for most of this work, we discuss results for $|z - Z| < 1$ m, while only in Section 5.5 we will examine briefly the impact of data for which $|z - Z| > 1$ m. With the notation $K_{eq}(R, \varphi, Z)$, we proceed now to derive the statistical moments for the two time periods.

5.2. Statistical Analysis of K_{eq}

We collected from the overall ensemble of signals only the ones obeying the requirement $|z - Z| < 1$ m and the remaining data points for early time period analysis are presented in Table 1. The number of contributing data points, that is, K_{eq} and $S_{s,eq}$ values for a given location, appears in each box corresponding to R and Z. It is emphasized that R assumes discrete values pertaining to couples of pumping and observation wells, the former from any of the three wells (A1, B1, and C1) and the latter from any of the seven wells (B3, C1, C2, C3, C4, C5, and C6, see Figure 2a). Altogether there are 16 values of R in Table 1, where we amalgamated the data originating from close values of R, within an interval smaller than 0.8 m and attributed R to the mean of each of the resulting 8 clusters. This explains the different number of data in Table 1 for the different R.

An additional cause of varying numbers of data points in Table 1 is the data filtering which was carried out. From the total number of 301 data points we filtered out those which could not be approximated by the homogeneous analytical solution (Equation 5) with an error smaller than 5% and those that resulted in outlier values of equivalent properties (see Section 3.3), leaving a total of 237 points. In total, about 21% of the signals were removed for the early time analysis to ensure that ambiguous data are not included. To guarantee that the removal of data does not have a significant impact on the results, we regenerated the results of Sections 5.2–5.4 with only the 5% criteria, which reduced the data points removed to only 8%. The results were very similar to the ones presented here without any significant change in values presented in Figures 7–10. Altogether, the contributing data points for a given R and Z presented in Table 1 differ from one another primarily due to the angle φ of the observation location.

We regard now the values of K_{eq} for a given R, differing in Z and φ (which are independent), as a random variable whose univariate CDF (cumulative distribution function) is illustrated in Figure 6a for $R = 9.6$ m. It is seen that $\ln K_{eq}$ is very accurately approximated by a normal distribution, that is, K_{eq} is lognormal. This plot is typical for the CDF considering other R values as well and therefore is representative of the entire $|z - Z| < 1$ m data set. The low value of $\sigma^2_{\ln Keq} \cong 0.08$ indicates that the Boise aquifer is weakly heterogeneous; in particular, in such a case a property of the lognormal distribution is $\mathrm{CV}^2 = \sigma^2_{Keq}/\langle K_{eq}\rangle^2 \cong \sigma^2_{\ln Keq}$, where CV is the coefficient of variation.

Table 1
Number of Data Points (After Filtering) for Early Time Period Analysis, Considering Each Pumping Elevation Z and Observation Location R (Within 0.8 m of Specified Values) and for $|z - Z| < 1$ m

Z (m)\R (m)	4.2	6.1	7.3	8.4	9.6	12.4	14.2	17.1	
−2	0	1	0	2	1	0	0	0	
−4	0	12	2	7	10	8	2	3	
−6	0	4	2	4	11	6	2	2	
−8	1	4	3	4	11	6	2	2	
−10	1	7	4	6	11	6	2	2	
−12	2	8	4	6	12	5	1	2	
−14	2	6	2	6	9	2	2	2	
−16	0	1	1	3	6	2	1	1	
Total	6	43	18	38	71	35	12	14	237

For each R in Table 1, the mean $\langle K_{eq}\rangle$ is calculated by averaging overall data differing in Z and φ. The result is plotted in Figure 7a as a function of R. Furthermore, we applied the same procedure to the data pertinent to the late time period using the homogeneous solution of Equation (6). A table similar to Table 1, with a similar distribution of data among the 8 values of R (with a total number of 235 data points remaining after filtering), is not reproduced here for brevity. These K_{eq} values differing in Z and φ are also averaged and the results for $\langle K_{eq}\rangle$ in both time periods are presented in Figure 7a, which is one of the main results of the present study. To emphasize the different numbers of contributing data, the symbols are of different sizes, proportional to the number of data. Thus, it is seen in Table 1 that the maximal number contributing to the early period is 71 for $R = 9.6$ m, while the minimal are 6 and 12–14 for the extreme $R_{min} = 4.2$ m and $R_{max} = 14.2$–17.1 m, respectively. The corresponding numbers for the late period are 61, 8, and 10 for the same R values.

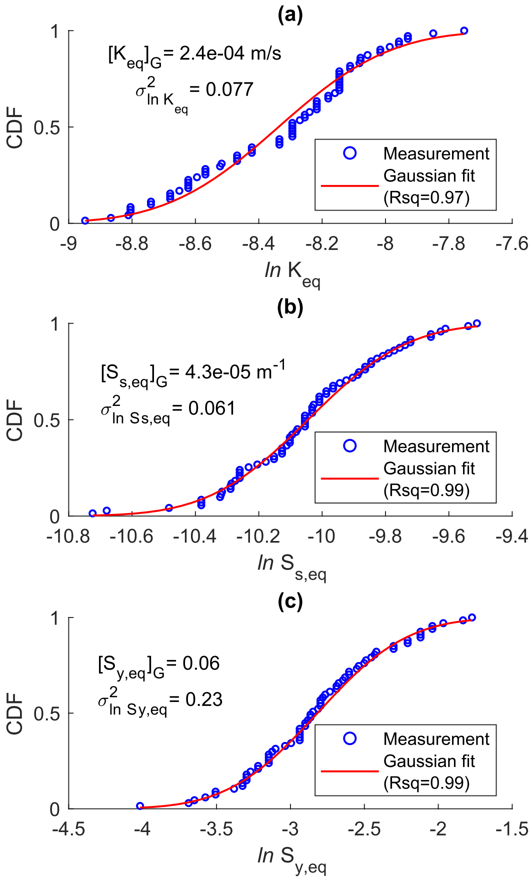

Figure 6. Cumulative density functions of (a) $\ln K_{eq}$, (b) $\ln S_{s,eq}$, and (c) $\ln S_{y,eq}$, for all data points with $R = 9.6$ m (71 points for early time period, see Table 1). A Gaussian cumulative distribution function is fitted for comparison with mean and variance specified for each plot.

Inspection of Figure 7a reveals that $\langle K_{eq}\rangle$ values based on the early and late period are very similar, that is, the results are consistent between the two different analyses. This is in line with the result presented in Figure 4 for K_{eq}, considering a specific data point rather than the average. It is an encouraging result, since the mechanisms of water release from elastic storage and water table drop and the respective homogeneous solutions (Equations 5 and 6) are completely different, yet the results are similar, indicating robustness of our $\langle K_{eq}\rangle$ estimation. Furthermore, in line with the steady-state theoretical results discussed above, $\langle K_{eq}\rangle$ decreases with increasing R, and appears to level off at the largest R, presumably reaching the limit $K_{efu} \cong 1.7 \times 10^{-4}$ m/s (expected to represent a lower bound of the horizontal conductivity if we take into account anisotropy). The maximal value at $R_{\min} = 4.2$ m is $\langle K_{eq}\rangle \cong 3.7 \times 10^{-4}$ m/s and the relatively small differences between minimal and maximal R stems from the weak heterogeneity of the BHRS aquifer. The range of estimated $\langle K_{eq}\rangle$ seen in Figure 7a is compared with previous results from the literature in the summarizing Table 2. It can be seen that the estimated values are within the lower part of the range of previous literature values and the overall average of 2.4×10^{-4} m/s is in good agreement with the literature average discussed in Section 3.1 of 3.8×10^{-4} m/s.

Figure 7a also presents error bars on each of the $\langle K_{eq}\rangle$ values for the early time period. These are obtained by calculating the variance (corresponding to Figure 7b) and taking the error bar to be two standard deviations below and above the average, in a typical fashion for uncertainty analysis. The uncertainty expressed by the error bars is not only an expression of the heterogeneity but also includes any other sources of variability such as measurement errors (head, depth, distance, etc.) and other sources of model errors or aquifer variability (aquifer depth, water table elevation, pumping onset, etc.). It can be seen that even considering uncertainties, the conclusions discussed above regarding the trend and range of $\langle K_{eq}\rangle$ values do not change. The error bars are generally small, except for the first $\langle K_{eq}\rangle$ value, closest to the well. However, for this value, the corresponding error bar for late time period (not shown in the figure) is much smaller, which may indicate a less reliable data set for early time period. We expect that the most significant part of the uncertainty is related to heterogeneity and not other factors. To test this hypothesis, we have also conducted a sensitivity analysis to evaluate the impact of the main parameters on the results of Figure 7. We first tested the impact of a 10% error in the depth of the aquifer D, that is, adding or subtracting from the elevation of the aquifer bottom (keeping the top constant). Results showed that there was only a minor change of around 10% on the $\langle K_{eq}\rangle$ values. Similar results were obtained when varying the elevation of the top of the aquifer (keeping the bottom constant) and when changing the pumping discharge Q.

Subsequently, we have calculated the squared coefficient of variation of K_{eq}, that is, $\sigma^2_{Keq}/\langle K_{eq}\rangle^2$ for the two time periods and the outcome is displayed in Figure 7b. It is seen that, again, in line with the steady-state theoretical results, for example, Bellin et al. (2020) (see their Figure 5), $\sigma^2_{Keq}/\langle K_{eq}\rangle^2$ decreases with R, but the tendency is not as clear as the one of $\langle K_{eq}\rangle$ (Figure 7a). For large R, the value of $\sigma^2_{Keq}/\langle K_{eq}\rangle^2 \cong 0.06$ in Figure 7b indicates that, as expected, the presumed K_{efu} is practically deterministic, that is, hardly varying in space. The average $\sigma^2_{Keq}/\langle K_{eq}\rangle^2 \cong 0.1$ over R can be regarded as representative for the weakly heterogeneous BHRS aquifer. We note that the literature values for $\sigma^2_{Keq}/\langle K_{eq}\rangle^2$ listed in Table 2 regard K variation and not K_{eq} variation and therefore should not be directly compared with our results. While the K_{eq} variance is expected to approach zero for large R, as $K_{eq} \rightarrow K_{efu}$, the overall K variance is a constant which previous literature considers to be $\sigma^2_{\ln K} = 0.49$. The fact that equivalent properties are less variable than the point values and their variance diminish with R are consequences of the implied space averaging over the distance between the source and the observation point. Future work of deriving theoretical expressions for equivalent properties, as mentioned in the second step in the Introduction, may clarify the relationship between $\sigma^2_{\ln Keq}$ and $\sigma^2_{\ln K}$.

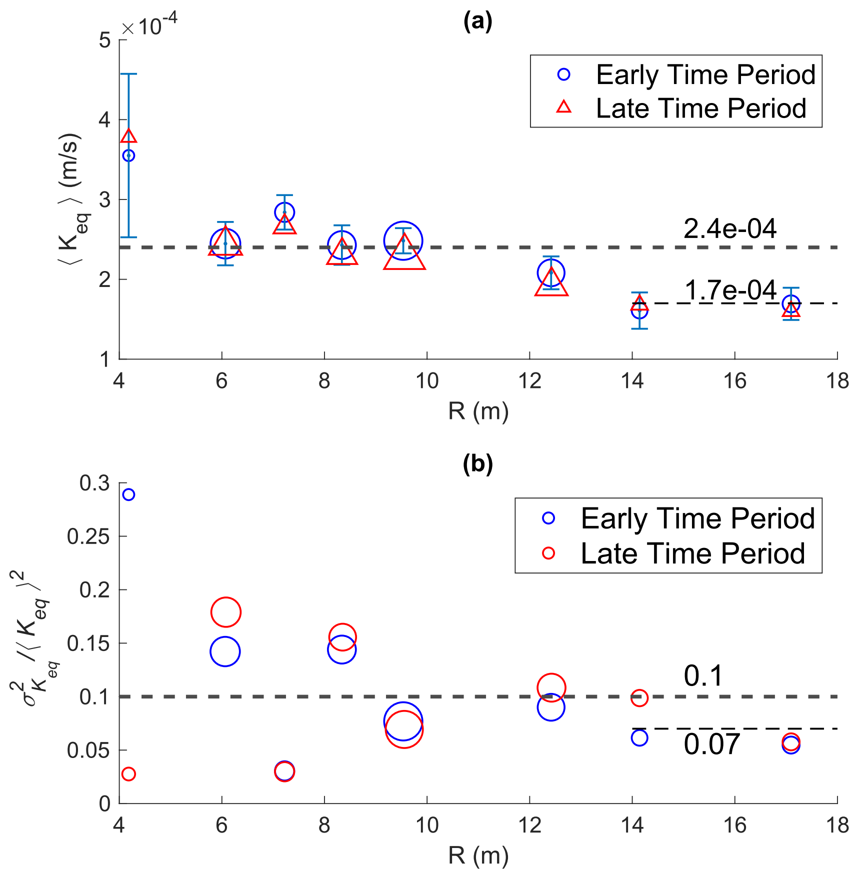

Figure 7. (a) Average equivalent conductivity and (b) squared coefficient of variation of K_{eq} as a function of horizontal distance R from the pumping interval. Symbol size corresponds to the number of data points which were averaged (see Table 1 for early time). Averages for all values and for the two largest R values are indicated on the plot with dashed lines.

5.3. Statistical Analysis of $S_{s,eq}$

It is customary to assume that specific storage of aquifers is much less variable than the hydraulic conductivity. Such an assumption was justified for instance by Dagan (1989, Section 3.2.1) on the basis of the linear relationship proposed by Freeze (1975) between $\ln S_s$ and $\ln K$. It led to the conclusion that $\sigma^2_{\ln S_s}$ is smaller by an order of magnitude than $\sigma^2_{\ln K}$. Tomographic tests offer an opportunity to examine this topic in a more profound manner and this was exactly the focus of the recent work by Zhao and Illman (2021), which studies the impact of S_s variability in HT. It differs from the present study in both methodology and cases considered (2D sand box and a synthetic aquifer). In any case, they found that S_s variability is not negligible and its impact on flow field is regarded a topic of future investigation. Our more limited aim at present is to examine the behavior of the mean and variance of $S_{s,eq}$ for the BHRS, along the lines of the previous section.

As indicated previously, in the early time period, for each value of K_{eq}, a parallel value of $S_{s,eq}$ was identified by fitting the homogeneous solution of Equation 5. Thus, the number of data depending on R, φ, and Z are exactly the same as the ones displayed in Table 1, discussed previously for K_{eq}. Proceeding along the same line as before, we illustrate first a typical CDF of $\ln S_s$ in Figure 6b, taken from the data at $R = 9.6$ m. It is seen that $\ln S_{s,eq}$ is fitted by a normal distribution with high accuracy, similar to what was observed for $\ln K_{eq}$ (Figure 6a). Furthermore, it is weakly heterogeneous, with variance $\sigma^2_{\ln S_{s,eq}} = 0.061$, which is close to that found for conductivity ($\sigma^2_{\ln K_{eq}} = 0.071$).

A more complete picture is offered by the dependence of $\langle S_{s,eq}\rangle$ upon R, displayed in Figure 8a. It is seen that it follows the same pattern as $\langle K_{eq}\rangle$, decreasing with larger R and stabilizing, apparently, at the "effective" value of 2.1×10^{-5} 1/m, while the overall mean over R is 4×10^{-5} 1/m. However, unlike the behavior of $\langle K_{eq}\rangle$, there is

Table 2
Comparison of Literature Boise Hydrogeophysical Research Site Property Values and the Values From the Results of This Work

Aquifer properties	Literature values	$R_{min} = 4.2$ m	Averaged over R	$R_{max} = 17.1$ m
$\langle K_{eq}\rangle$ (m/s)	$1.5 - 8.9 \times 10^{-4}$ (a,b)	3.7×10^{-4}	2.4×10^{-4}	1.7×10^{-4}
$\langle S_{s,eq}\rangle$ (1/m)	$0.25 - 9.8 \times 10^{-5}$ (c,d)	5.9×10^{-5}	4×10^{-5}	2.1×10^{-5}
$\langle S_{y,eq}\rangle$*	0.01–0.06 (d)	0.08	0.06	0.04
$\sigma^2_{K_{eq}}/\langle K_{eq}\rangle^2$	0.36 – 0.92 (a)**	0.17	0.1	0.07
$\sigma^2_{S_{s,eq}}/\langle S_{s,eq}\rangle^2$	n/a	0.16	0.08	0.02
$\sigma^2_{S_{y,eq}}/\langle S_{y,eq}\rangle^2$	n/a	0.34	0.19	0.09

Note. Literature: (a) Cardiff, Barrash, and Kitanidis (2013), (b) Barrash and Cardiff (2013), (c) Rabinovich et al. (2015), and (d) Barrash et al. (2006). * Similarly low S_y values from analytical modeling of aquifer tests have been reported by numerous workers (e.g., Chen & Ayers, 1998; Moench, 1994). ** The literature values given here are for variance of pointwise $\ln K$ and not for squared coefficient of variation of K_{eq}.

no theoretical model for $\langle S_{s,eq}\rangle$ to compare with. The values seen in Figure 8a are summarized in Table 2, where it can be seen that they are within the range of literature values for the BHRS. The average over R is in excellent agreement with the overall literature value of 3.8×10^{-5} 1/m discussed in Section 3.1. Error bars in Figure 8a show that even considering uncertainties, these conclusions do not change significantly. The increase in size of the error bars with smaller R values maybe associated with the impact of heterogeneity. Finally, the dependence

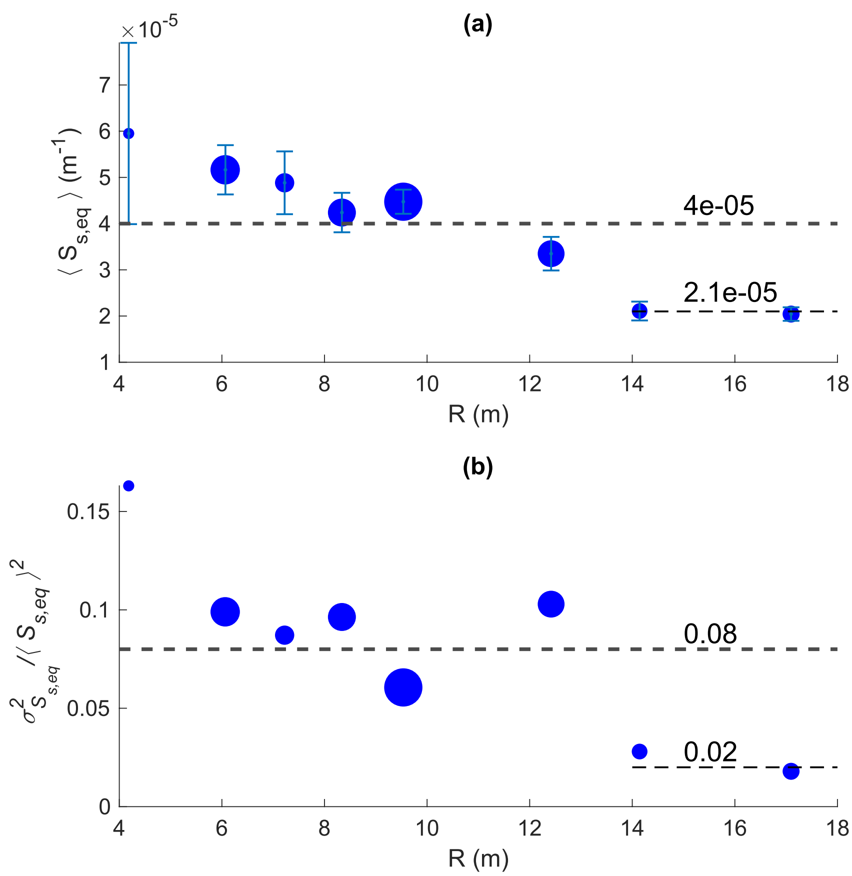

Figure 8. (a) Average equivalent specific storage and (b) squared coefficient of variation of $S_{s,eq}$ as a function of horizontal distance R from the pumping interval. Symbol size corresponds to the number of data points which where averaged (see Table 1). Averages for all values and for the two largest R values are indicated on the plot with dashed lines.

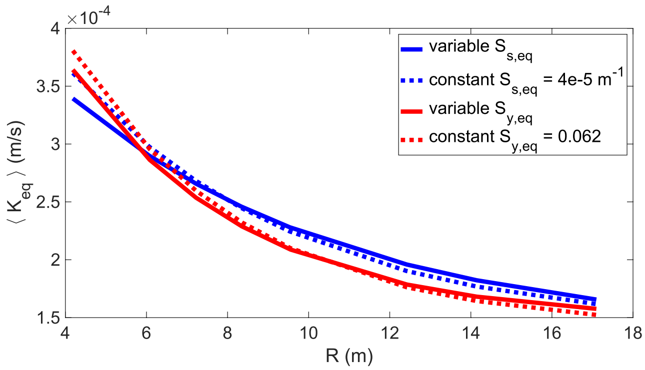

Figure 9. Mean K_{eq} as a function of horizontal distance R considering constant $S_{s,eq}$ and $S_{y,eq}$ values, that is, fitting Equations 5 and 6 to data seeking only a single variable K_{eq}. Lines are exponential fits to the data points and previous results (variable $S_{s,eq}$, $S_{y,eq}$) are plotted for comparison.

of $\sigma^2_{Ss,eq}/\langle S_{s,eq}\rangle^2$ upon R is displayed in Figure 8b. Again, its mean over R is equal to 0.08, that is, weak heterogeneity, and it drops to about 0.02 for large R, indicating that indeed $\langle S_{s,eq}\rangle$ is an "effective" value.

Future investigations are expected to provide a theoretical foundation for these properties of spatially variable S_s. Still, we wish to examine the impact of assuming that S_s is constant upon the identification of $\langle K_{eq}\rangle$, as was customarily done in the literature. Toward this aim, we have fitted the homogeneous solution of Equation 5 to the observed signals with fixed $S_s = 4 \times 10^{-5}$ 1/m, leaving K_{eq} as the only variable to be identified. It is emphasized that in order to maintain the same number of data sets as presented in Table 1, it was necessary to relax the fitting error (Equation 7) tolerance from 5% for variable $S_{s,eq}$ to 20% for fixed $S_{s,eq}$. In Figure 9, we compare the dependence of $\langle K_{eq}\rangle$ upon R for variable and fixed $S_{s,eq}$ to find out that the results are very close, justifying the usual assumption of constant S_s when identifying K_{eq}, at least for the weak heterogeneity of the BHRS. We also checked the possible correlation between K_{eq} and $S_{s,eq}$ by plotting the residuals of the two; the points were scattered with no apparent correlation. This result is in line with the conclusions presented in the recent review paper by Kuang et al. (2020).

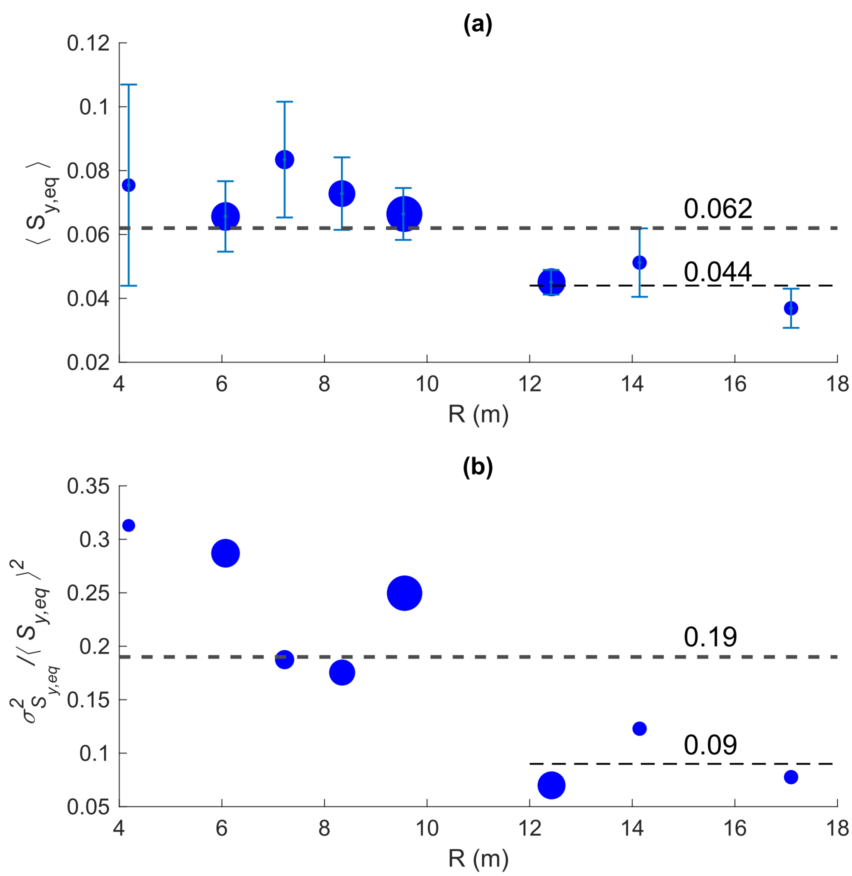

Figure 10. (a) Average equivalent specific yield and (b) squared coefficient of variation of $S_{y,eq}$ as a function of horizontal distance R from the pumping interval. Symbol size corresponds to the number of data points which where averaged. Averages for all values and for the two largest R values are indicated on the plot with dashed lines.

5.4. Statistical Analysis of $S_{y,eq}$

We move now to the analysis of the equivalent specific yield identified in the late time period by the use of the homogeneous solution of Equation 6. The solution is fitted to the observed head signals, with the total number of data points being 235, after a similar filtering as the one applied for the early time analysis. We illustrate first the CDF of $\ln S_{y,eq}$ for the same $R = 9.6$ m in Figure 6c. It is seen that $\ln S_{y,eq}$ is fitted accurately by a normal distribution, similar to $\ln K_{eq}$ (Figure 6a). Furthermore, it is weakly heterogeneous, with variance $\sigma^2_{\ln S_{y,eq}} = 0.23$, which is however larger than the ones characterizing the other two parameters ($\sigma^2_{\ln K_{eq}} = 0.077$ and $\sigma^2_{\ln S_{s,eq}} = 0.061$).

The overall behavior is illustrated by the dependence of $\langle S_{y,eq} \rangle$ upon R in Figure 10a. Again, there is a tendency of drop with R; similar to $\langle S_{s,eq} \rangle$ and there is no theoretical work to support this behavior yet. However, large error bars can be seen indicating that the observed trend maybe in question. The overall mean value over R is $\langle S_{s,eq} \rangle = 0.062$ whereas the value pertinent to large R is $\langle S_{s,eq} \rangle \cong 0.04$. The values seen in Figure 10a are summarized in Table 2, where it can be seen that they are mostly within the range of literature values for the BHRS. The average over R is in agreement with the overall literature value of 0.028 discussed in Section 3.1. The dependence of $\sigma^2_{S_{y,eq}} / \langle S_{s,eq} \rangle^2$ upon R is presented in Figure 10b, where a tendency to decrease with R is seen, the mean value over R being 0.19, while the value at large R is about 0.1. Thus, the equivalent specific yield is subjected to a larger uncertainty than the equivalent conductivity and specific storage and its "effective" value maybe somewhat smaller than 0.04. This is also supported by the large error bars in Figure 10a.

Finally, we checked again the impact of the common assumption of constant and deterministic S_y, that is, S_y is assumed constant in space and having a known value. Substituting $S_y = 0.062$ in the homogeneous solution of Equation 6 leaves only K_{eq} as the variable to be identified from best fitting with observations. To maintain the number of data points as the one for variable $S_{y,eq}$, the error tolerance in the fitting (Equation 7) was increased slightly to 7%. In Figure 9, we compare the dependence of $\langle K_{eq} \rangle$ upon R for variable and fixed $S_{y,eq}$ and the results are very close, justifying again the usual assumption of constant S_y when identifying K_{eq} for the BHRS.

5.5. Extension to $|z - Z| \neq 0$

As a first attempt to grasp the impact of measurement head signals with a vertical offset, that is, $|z - Z|$ larger than 1 m, we fitted the homogeneous solutions of Equations 5 and 6 to measured signals $H_Z(R, \varphi, z, t)$ in order to identify the corresponding K_{eq}, $S_{s,eq}$, and $S_{y,eq}$. Toward this aim, we considered for each source at Z (Figure 2b) the observation points within bands of 2 m thickness centered at $|z - Z| = 2$, 4, and 6 m (the previous analysis of $|z - Z| < 1$ is now denoted $|z - Z| = 0$). It is emphasized that due to the presence of boundaries the number of available data decrease with increasing $|z - Z|$ and for this reason we limited the offset to 6 m. Furthermore, for a fixed $|z - Z|$ and R the independent variable is now $r = \left[R^2 + (z - Z)^2\right]^{1/2}$, such that for a homogeneous and unbounded medium the properties are constant.

We have represented in Figure 11 the dependence of $\langle K_{eq} \rangle$ upon r for early time (Figure 11a) and late time (Figure 11b) analysis, as well as $\langle S_{s,eq} \rangle$ (Figure 11c) and $\langle S_{y,eq} \rangle$ (Figure 11d) variation with r. All plots show results for $|z - Z| = 0$ (the previous results for which $r = R$) and also for $|z - Z| = 2$, 4, and 6 m separately. The averaging was carried out as before by regarding Z and φ as independent variables. It is seen in Figures 11a–11d that there is no clear trend differentiating data points for different $|z - Z|$, except maybe for the smallest r, that is, the results for $|z - Z| \neq 0$ are very similar to the $|z - Z| = 0$ results. Although this is a preliminary analysis, the results indicate that the selection of dependence of the mean and variance of equivalent properties upon R for $|z - Z| = 0$ in the preceding sections is a representative one. Future work incorporating the impact of statistical anisotropy may build on and increase our understanding of the results for $|z - Z| \neq 0$.

6. Summary and Conclusions

The tomography pumping test conducted in 2011 at the BHRS offers a unique opportunity to carry out statistical analysis of the aquifer properties by virtue of the systematic testing and large amounts of data collected at many locations distributed throughout the site. In this work, we adopt an approach for tomography pumping test analysis by which the statistical moments of equivalent properties are calculated. This approach does not offer a pointwise estimation (e.g., conductivity map) of the properties, as advanced by many HT studies in previous

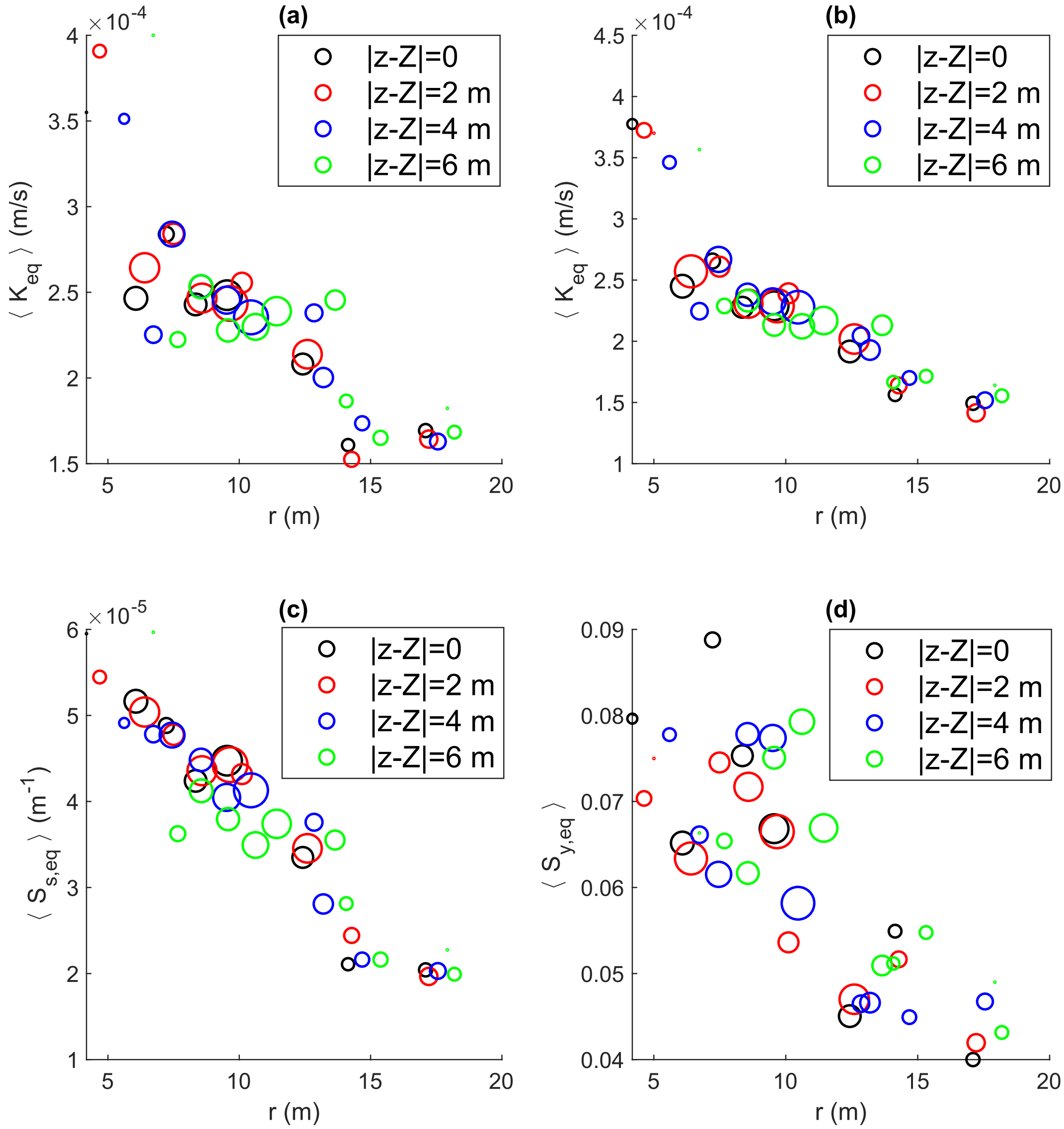

Figure 11. (a) Average equivalent conductivity for early time period analysis, (b) average equivalent conductivity for late time period analysis, (c) average equivalent specific storage, and (d) average equivalent specific yield as a function of r considering measurement head data at different bands of $|z - Z| = 0, 2, 4, 6$ m.

literature. However, it has the advantage of simplicity, requiring much less computational efforts and avoiding the ambiguities of the HT inverse problems. The BHRS is a phreatic aquifer, which allows us in this work to apply the analysis approach for calculation of the first two moments of K_{eq}, $S_{s,eq}$, and $S_{y,eq}$.

An additional advantage of the approach advanced here is that due to the robustness of the results for the mean properties, for example, $\langle K_{eq} \rangle$ as reflected by the low CV (Figure 7b) and by the density of points defining the CDF (Figure 6a), it is expected that similar results could be obtained by a smaller amount of data than typically employed for HT analyses. This topic could be examined in a systematic manner by gradually eliminating data and observing the effect, which is part of our plan for future studies.

Equivalent properties are relatively simple to calculate, requiring a match of the head data measured at a single location to a homogeneous aquifer solution. Intuitively, this property represents its varying values in the region between the pumping source and the measurement location. The possibility of using semianalytical solutions rather than numerical simulations for calculating equivalent properties contributes to the simplicity and efficiency of the process. In this work, we presented a novel approach for equivalent property calculation by matching two separate semianalytical solutions to the measured data, one for early time (elastic aquifer, neglecting S_y) and the other for a late time period (phreatic aquifer, neglecting S_s). This approach has some advantages over matching the full measured head signal, as discussed in Section 4.3, namely the requirement to solve an inverse problem with only two unknown variables instead of three. We apply this method to the BHRS data and calculate K_{eq}, $S_{s,eq}$ for early time period (roughly $t < 50$ s) and K_{eq}, $S_{s,eq}$ for late time period (roughly $t > 200$ s). The homogeneous solutions fit the data well, with many hundreds of signals having errors less than the chosen threshold of 5%.

Having calculated the spatial variation of K_{eq}, $S_{s,eq}$, and $S_{y,eq}$, we observe that the aquifer is heterogeneous, as expected, and continue by calculating their first two statistical moments. We first consider only observation points which are approximately in the same vertical location of the pumping segment ($|z - Z| < 1$) and therefore equivalent properties for a given R depend only on Z and φ. Plotting their CDFs for a given R, we find that all three properties are lognormally distributed with relatively small variances indicating weak heterogeneity (Figure 6). By exchanging ensemble averaging with spatial averaging, we calculate the mean and CV squared of each equivalent property as a function of R.

Results of field data analysis cannot be easily validated; however, the method developed here and the many previous investigations of the BHRS allowed for a validation of the results, at least to some extent. First, the early and late period results were compared and the excellent agreement shows that the results for K_{eq} are robust. Then a comparison with literature values showed that the results for effective properties found here are in the same range as those reported previously (see Table 2). Finally, due to the weak heterogeneity, all values of average K_{eq} varying with distance from the pumping well were also found to be close to the literature values.

The main result of this work is $\langle K_{eq} \rangle$ as a function of R (Figure 7) for the range $4.2 \leq R \leq 17.1$ m. We find that $\langle K_{eq} \rangle$ decreases with R and appears to converge to a constant value for large R, in agreement with previously published theory for the steady-state case (Indelman et al., 1996), which found that values vary from the arithmetic mean of K near the well to the uniform flow effective K (K_{efu}) far from the well. Furthermore, values were found to decrease from 2.4×10^{-4} m/s to 1.65×10^{-4} m/s, and this range is in agreement with the lower part of the range of previously published literature values as seen in Table 2. Finally, these results were obtained in two independent calculations, based on early time and late time periods of the data set. The consistency between the two calculations is an indication of the accuracy of the results.

Results for squared CV of K_{eq} are similar to $\langle K_{eq} \rangle$ in their dependence on R, with values indicating weak heterogeneity and decreasing to near zero values as K_{eq} converges to the constant K_{efu}. An analysis for $S_{s,eq}$ and $S_{y,eq}$ variation is presented here for the first time. It shows that they can be considered to be random variables as well, with a weak heterogeneity and a similar trend to that discussed for previous variables. Finally, we also show that similar results for K_{eq} are obtained when assuming constant $S_{s,eq}$ (for early time analysis) or constant $S_{y,eq}$ (for late time analysis). This suggests that the common approach, adopted by previous literature, of taking these aquifer parameters to be constants is a reasonable one.

The method for aquifer characterization and results presented in this work should be applicable to any small scale (i.e., tens of meters in R and $|z - Z|$) pumping test site. It is noted that we consider isotropic analytical solutions in our analysis; however, this can be easily extended to include anisotropy by adding an additional parameter to be identified and using the solutions for a homogeneous aquifer, for example, by Dagan (1967), Neuman (1974). Another expected extension of this work is deriving a semianalytical solution to the moments of equivalent properties as functions of those of the point values (see second step in the Introduction). This shall be done by a first order approximation for weakly heterogeneous aquifers subjected to unsteady pumping, which will then allow to identify the statistical moments of point value properties (see third step in Introduction), the ones most needed for applications to transport predictions. The third future work will be to estimate the impact of S_s and S_y heterogeneity on the flow, which is often thought to be negligible, despite the rather significant variability of these parameters found in this and other recent works (Zhao & Illman, 2021).

Data Availability Statement

The data from the tomography pumping test conducted in 2011 at the BHRS and used in this study are available at Zenodo via https://doi.org/10.5281/zenodo.7091457. The codes used for calculating the equivalent properties and generating the figures are also available there.

Acknowledgments

None.

References

Barrash, W., & Cardiff, M. (2013). Hydraulic conductivity distribution from multi-level slug tests and multivariate facies associations in a conglomeratic fluvial aquifer, Boise Hydrogeophysical Research Site. In *Boise Hydrogeophysical Research Site: Technical Report BSU CGISS, 13-03-v2020* (p. 70). Boise State University.

Barrash, W., & Clemo, T. (2002). Hierarchical geostatistics and multifacies systems: Boise Hydrogeophysical Research Site, Boise, Idaho. *Water Resources Research*, *38*(10), 14–21. https://doi.org/10.1029/2002wr001436

Barrash, W., Clemo, T., Fox, J., & Johnson, T. (2006). Field, laboratory, and modeling investigation of the skin effect at wells with slotted casing, Boise Hydrogeophysical Research Site. *Journal of Hydrology*, *326*(1), 181–198. https://doi.org/10.1016/j.jhydrol.2005.10.029

Barrash, W., & Reboulet, E. (2004). Significance of porosity for stratigraphy and textural composition in subsurface, coarse fluvial deposits: Boise Hydrogeophysical Research Site. *The Geological Society of America Bulletin*, *116*(9–10), 1059–1073. https://doi.org/10.1130/b25370.1

Bellin, A., Fiori, A., & Dagan, G. (2020). Equivalent and effective conductivities of heterogeneous aquifers for steady source flow, with illustration for hydraulic tomography. *Advances in Water Resources*, *142*, 103632. https://doi.org/10.1016/j.advwatres.2020.103632

Berg, S., & Illman, W. (2011). Three-dimensional transient hydraulic tomography in a highly heterogeneous glaciofluvial aquifer-aquitard system. *Water Resources Research*, *47*(10), W10507. https://doi.org/10.1029/2011wr010616

Binley, A., Keery, J., Slater, L., Barrash, W., & Cardiff, M. (2016). The hydrogeologic information in cross-borehole complex conductivity data from an unconsolidated conglomeratic sedimentary aquifer. *Geophysics*, *81*(6), E409–E421. https://doi.org/10.1190/geo2015-0608.1

Bohling, G. C., & Butler, J. J., Jr. (2010). Inherent limitations of hydraulic tomography. *Groundwater*, *48*(6), 809–824. https://doi.org/10.1111/j.1745-6584.2010.00757.x

Cardiff, M., Bakhos, T., Kitanidis, P., & Barrash, W. (2013). Aquifer heterogeneity characterization with oscillatory pumping: Sensitivity analysis and imaging potential. *Water Resources Research*, *49*(9), 5395–5410. https://doi.org/10.1002/wrcr.20356

Cardiff, M., & Barrash, W. (2011). 3-D transient hydraulic tomography in unconfined aquifers with fast drainage response. *Water Resources Research*, *47*(12), W12518. https://doi.org/10.1029/2010wr010367

Cardiff, M., Barrash, W., & Kitanidis, P. (2012). A field proof-of-concept of aquifer imaging using 3-D transient hydraulic tomography with modular, temporarily-emplaced equipment. *Water Resources Research*, *48*(5), W05531. https://doi.org/10.1029/2011wr011704

Cardiff, M., Barrash, W., & Kitanidis, P. (2013). Hydraulic conductivity imaging from 3-D transient hydraulic tomography at several pumping/observation densities. *Water Resources Research*, *49*(11), 7311–7326. https://doi.org/10.1002/wrcr.20519

Cardiff, M., Barrash, W., Kitanidis, P., Malama, B., Revil, A., Straface, S., & Rizzo, E. (2009). A potential-based inversion of unconfined steady-state hydraulic tomography. *Groundwater*, *47*(2), 259–270. https://doi.org/10.1111/j.1745-6584.2008.00541.x

Cardiff, M., Barrash, W., Thoma, M., & Malama, B. (2011). Information content of slug tests for estimating hydraulic properties in realistic, high-conductivity aquifer scenarios. *Journal of Hydrology*, *403*(1), 66–82. https://doi.org/10.1016/j.jhydrol.2011.03.044

Cardiff, M., Zhou, Y., Barrash, W., & Kitanidis, P. K. (2020). Aquifer imaging with oscillatory hydraulic tomography: Application at the field scale. *Groundwater*, *58*(5), 710–722. https://doi.org/10.1111/gwat.12960

Carrera, J., Alcolea, A., Medina, A., Hidalgo, J., & Slooten, L. (2005). Inverse problem in hydrogeology. *Hydrogeology Journal*, *13*(1), 206–222. https://doi.org/10.1007/s10040-004-0404-7

Carrera, J., & Neuman, S. (1986). Estimation of aquifer parameters under transient and steady state conditions: 1. Maximum likelihood method incorporating prior information. *Water Resources Research*, *22*(2), 199–210. https://doi.org/10.1029/wr022i002p00199

Carslaw, H., & Jaeger, J. (1959). *Conduction of heat in solids*. Oxford at Clarendon Press.

Chen, X., & Ayers, J. F. (1998). Aquifer properties determined from two analytical solutions. *Groundwater*, *36*(5), 783–791. https://doi.org/10.1111/j.1745-6584.1998.tb02196.x

Cheng, K., Dagan, G., & Rabinovich, A. (2020). Modeling diffusivity tests in heterogeneous aquifers: A stochastic first-order approach. *Water Resources Research*, *56*(9), e2020WR027672. https://doi.org/10.1029/2020wr027672

Cheng, K., Rabinovich, A., & Dagan, G. (2019). Stochastic modeling of oscillatory pumping in heterogeneous aquifers with application to Boise aquifer test. *Journal of Hydrology*, *569*, 278–290. https://doi.org/10.1016/j.jhydrol.2018.11.045

Clement, W., & Barrash, W. (2006). Crosshole radar tomography in a fluvial aquifer near Boise, Idaho. *Journal of Environmental & Engineering Geophysics*, *11*(3), 171–184. https://doi.org/10.2113/jeeg11.3.171

Clement, W., Barrash, W., & Knoll, M. (2006). Reflectivity modeling of a ground-penetrating-radar profile of a saturated fluvial formation. *Geophysics*, *71*(3), K59–K66. https://doi.org/10.1190/1.2194528

Clement, W., & Knoll, M. (2006). Traveltime inversion of vertical radar profiles. *Geophysics*, *71*(3), K67–K76. https://doi.org/10.1190/1.2194527

Dafflon, B., & Barrash, W. (2012). Three-dimensional stochastic estimation of porosity distribution: Benefits of using ground-penetrating radar velocity tomograms in simulated-annealing-based or Bayesian sequential simulation approaches. *Water Resources Research*, *48*(5), W05553. https://doi.org/10.1029/2011wr010916

Dafflon, B., Barrash, W., Cardiff, M., & Johnson, T. C. (2011). Hydrological parameter estimations from a conservative tracer test with variable-density effects at the Boise Hydrogeophysical Research Site. *Water Resources Research*, *47*(12), W12513. https://doi.org/10.1029/2011wr010789

Dafflon, B., Irving, J., & Barrash, W. (2011). Inversion of multiple intersecting high-resolution crosshole GPR profiles for hydrological characterization at the Boise Hydrogeophysical Research Site. *Journal of Applied Geophysics*, *73*(4), 305–314. https://doi.org/10.1016/j.jappgeo.2011.02.001

Dagan, G. (1966). Solution of linearized equations of free-surface flow in porous media. *Journal de Mecanique*, *5*(2), 207–215.

Dagan, G. (1967). A method Determining the permeability and effective porosity unconfined anisotropic aquifers. *Water Resources Research*, *34*(4), 1059–1072. https://doi.org/10.1029/wr003i004p01059

Dagan, G. (1989). *Flow and transport in porous formations*. Springer-Verlag.

Ernst, J., Green, A., Maurer, H., & Holliger, K. (2007). Application of a new 2D time-domain full-waveform inversion scheme to crosshole radar data. *Geophysics*, *72*(5), J53–J64. https://doi.org/10.1190/1.2761848

Freeze, R. A. (1975). A stochastic-conceptual analysis of one-dimensional groundwater flow in nonuniform homogeneous media. *Water Resources Research*, *11*(5), 725–741. https://doi.org/10.1029/WR011i005p00725

Gottlieb, J., & Dietrich, P. (1995). Identification of the permeability distribution in soil by hydraulic tomography. *Inverse Problems*, *11*(2), 353–360. https://doi.org/10.1088/0266-5611/11/2/005

Hantush, M. S. (1961). Drawdown around a partially penetrating well. *Journal of the Hydraulics Division*, *87*(4), 83–98. https://doi.org/10.1061/jyceaj.0000633

Hochstetler, D., Barrash, W., Leven, C., Cardiff, M., Chidichimo, F., & Kitanidis, P. (2016). Hydraulic tomography: Continuity and discontinuity of high-k and low-k zones. *Groundwater*, *54*(2), 171–185. https://doi.org/10.1111/gwat.12344

Indelman, P. (2001). Steady-state source flow in heterogeneous porous media. *Transport in Porous Media*, *45*(1), 105–127. https://doi.org/10.1023/a:1011814418142

Indelman, P., Fiori, A., & Dagan, G. (1996). Steady flow toward wells in heterogeneous formations: Mean head and equivalent conductivity. *Water Resources Research*, *32*(7), 1975–1983. https://doi.org/10.1029/96wr00990

Irving, J., Knoll, M., & Knight, R. (2007). Improving crosshole radar velocity tomograms: A new approach to incorporating high-angle traveltime data. *Geophysics*, *72*(4), J31–J41. https://doi.org/10.1190/1.2742813

Kitanidis, P., & Vomvoris, E. (1983). A geostatistical approach to the inverse problem in groundwater modeling (steady state) and one-dimensional simulations. *Water Resources Research*, *19*(3), 677–690. https://doi.org/10.1029/wr019i003p00677

Kroszynski, U. (1975). Flow in a vertical porous column drained at its bottom at constant flux. *Journal of Hydrology*, *24*(1–2), 135–153. https://doi.org/10.1016/0022-1694(75)90147-x

Kroszynski, U., & Dagan, G. (1975). Well pumping in unconfined aquifers: The influence of the unsaturated zone. *Water Resources Research*, *11*(3), 479–490. https://doi.org/10.1029/wr011i003p00479

Kuang, X., Jiao, J. J., Zheng, C., Cherry, J. A., & Li, H. (2020). A review of specific storage in aquifers. *Journal of Hydrology*, *581*, 124383. https://doi.org/10.1016/j.jhydrol.2019.124383

Malama, B., & Johnson, B. (2010). Analytical modeling of saturated zone head response to evapotranspiration and river-stage fluctuations. *Journal of Hydrology*, *382*(1–4), 1–9. https://doi.org/10.1016/j.jhydrol.2009.12.010

Malama, B., Kuhlman, K., Barrash, W., Cardiff, M., & Thoma, M. (2011). Modeling slug tests in unconfined aquifers taking into account water table kinematics, wellbore skin and inertial effects. *Journal of Hydrology*, *408*(1–2), 113–126. https://doi.org/10.1016/j.jhydrol.2011.07.028

Mao, D., Wan, L., Yeh, T.-C. J., Lee, C.-H., Hsu, K.-C., Wen, J.-C., & Lu, W. (2011). A revisit of drawdown behavior during pumping in unconfined aquifers. *Water Resources Research*, *47*(5), W05502. https://doi.org/10.1029/2010wr009326

Matheron, G. (1967). *Eléments pour une théorie des milieux poreux*. Masson.

Moench, A. F. (1994). Specific yield as determined by type-curve analysis of aquifer-test data. *Groundwater*, *32*(6), 949–957. https://doi.org/10.1111/j.1745-6584.1994.tb00934.x

Moret, G., Clement, W., Knoll, M., & Barrash, W. (2004). VSP traveltime inversion: Near-surface issues. *Geophysics*, *69*(2), 345–351. https://doi.org/10.1190/1.1707053

Moret, G., Knoll, M., Barrash, W., & Clement, W. (2006). Investigating the stratigraphy of an alluvial aquifer using crosswell seismic traveltime tomography. *Geophysics*, *71*(3), B63–B73. https://doi.org/10.1190/1.2195487

Mwenifumbo, C., Barrash, W., & Knoll, M. (2009). Capacitive conductivity logging and electrical stratigraphy in a high-resistivity aquifer, Boise Hydrogeophysical Research Site. *Geophysics*, *74*(3), E125–E133. https://doi.org/10.1190/1.3106760

Neuman, S. (1974). Effect of partial penetration on flow in unconfined aquifers considering delayed gravity response. *Water Resources Research*, *10*(2), 313–312. https://doi.org/10.1029/wr010i002p00303

Neuman, S., & Yakowitz, S. (1979). A statistical approach to the inverse problem of aquifer hydrology: 1. Theory. *Water Resources Research*, *15*(4), 845–860. https://doi.org/10.1029/wr015i004p00845

Rabinovich, A., Barrash, W., Cardiff, M., Hochstetler, D., Bakhos, T., Dagan, G., & Kitanidis, P. (2015). Frequency dependent hydraulic properties estimated from oscillatory pumping tests in an unconfined aquifer. *Journal of Hydrology*, *531*, 2–16. https://doi.org/10.1016/j.jhydrol.2015.08.021

Schwartz, F. W., & Zhang, H. (2003). *Fundamentals of groundwater* (p. 583). John Wiley & Sons.

Straface, S., Chidichimo, F., Rizzo, E., Riva, M., Barrash, W., Revil, A., et al. (2011). Joint inversion of steady-state hydrologic and self-potential data for 3D hydraulic conductivity distribution at the Boise Hydrogeophysical Research Site. *Journal of Hydrology*, *407*(1–4), 115–128. https://doi.org/10.1016/j.jhydrol.2011.07.013

Tartakovsky, G., & Neuman, S. (2007). Three-dimensional saturated-unsaturated flow with axial symmetry to a partially penetrating well in a compressible unconfined aquifer. *Water Resources Research*, *43*(1), W01410. https://doi.org/10.1029/2006wr005153

Theis, C. V. (1935). The relation between the lowering of the piezometric surface and the rate and duration of discharge of a well using ground-water storage. *Eos, Transactions American Geophysical Union*, *16*(2), 519–524. https://doi.org/10.1029/tr016i002p00519

Tiedeman, C., & Barrash, W. (2020). Hydraulic tomography: 3D hydraulic conductivity, fracture network, and connectivity in mudstone. *Groundwater*, *58*(2), 238–257. https://doi.org/10.1111/gwat.12915

Tronicke, J., Holliger, K., Barrash, W., & Knoll, M. (2004). Multivariate analysis of cross-hole georadar velocity and attenuation tomograms for aquifer zonation. *Water Resources Research*, *40*(1), W01519. https://doi.org/10.1029/2003wr002031

Wu, C.-M., Yeh, T.-C. J., Zhu, J., Lee, T. H., Hsu, N.-S., Chen, C.-H., & Sancho, A. F. (2005). Traditional analysis of aquifer tests: Comparing apples to oranges? *Water Resources Research*, *41*(9), W09402. https://doi.org/10.1029/2004wr003717

Yeh, H.-D., Huang, C., Chang, Y., & Jeng, D. (2010). An analytical solution for tidal fluctuations in unconfined aquifers with a vertical beach. *Water Resources Research*, *46*(10), WR008746. https://doi.org/10.1029/2009wr008746

Yeh, T., Jin, M., & Hanna, S. (1996). An iterative stochastic inverse method: Conditional effective transmissivity and hydraulic head fields. *Water Resources Research*, *32*(1), 85–92. https://doi.org/10.1029/95wr02869

Yustres, A., Asensio, L., Alonso, J., & Navarro, V. (2012). A review of Markov Chain Monte Carlo and information theory tools for inverse problems in subsurface flow. *Computational Geosciences*, *16*(1), 1–20. https://doi.org/10.1007/s10596-011-9249-z

Zarlenga, A., Janković, I., Fiori, A., & Dagan, G. (2018). Effective hydraulic conductivity of three-dimensional heterogeneous formations of lognormal permeability distribution: The impact of connectivity. *Water Resources Research*, *54*(3), 2480–2486. https://doi.org/10.1002/2017wr022141

Zha, Y., Yeh, T.-C. J., Illman, W. A., Zeng, W., Zhang, Y., Sun, F., & Shi, L. (2018). A reduced-order successive linear estimator for geostatistical inversion and its application in hydraulic tomography. *Water Resources Research*, *54*(3), 1616–1632. https://doi.org/10.1002/2017wr021884

Zhao, Z., & Illman, W. A. (2021). On the importance of considering specific storage heterogeneity in hydraulic tomography: Laboratory sandbox and synthetic studies. *Journal of Hydrology*, *593*, 125874. https://doi.org/10.1016/j.jhydrol.2020.125874